COMPUTATIONAL EME COMPLIANCE ASSESSMENT OF MOBILE RADIO MODEL M30TXS9PW1AN (MHUS1009A)

September 29, 2011

Giorgi Bit-Babik, Ph.D., and Antonio Faraone, Ph.D.

Motorola Corporate EME Research Lab, Plantation, Florida

Introduction

This report summarizes the computational [numerical modeling] analysis performed to document compliance of the APX7500 Dual Band UHFR1 and 7/800MHz, Model Number M30TXS9PW1AN (MHUS1009A), mobile radio and vehicle-mounted antennas with the Federal Communications Commission (FCC) guidelines for human exposure to radio frequency (RF) emissions. The radio operates in the 380 - 470 MHz and 7/800 MHz frequency bands.

This computational analysis supplements the measurements conducted to evaluate the compliance of the exposure from this mobile radio with respect to applicable *maximum permissible exposure* (MPE) limits. All test conditions (27 in total) that did not conform with applicable MPE limits were analyzed to determine whether those conditions complied with the *specific absorption rate* (SAR) limits for general public exposure (1.6 W/kg averaged over 1 gram of tissue and 0.08 W/kg averaged over the whole body) set forth in FCC guidelines, which are based on the IEEE C95.1-1999 standard [1]. In total 52[1] independent simulations have been performed. Thirty two simulations are addressing exposure of passenger and another twenty simulations are addressing exposure of bystander to the UHF mobile radios with trunk-mount antennas. For all simulations a commercial code based on Finite-Difference-Time-Domain (FDTD) methodology was employed to carry out the computational analysis. It is well established

[1] The number of individual simulations includes: 20 bystander simulations (the front and back bystander orientations in 10 test conditions), 30 passenger simulations (the center and side location at the back seat in 15 test conditions), and 2 passenger simulations in the front seat location.

and recognized within the scientific community that SAR is the primary dosimetric quantity used to evaluate the human body's absorption of RF energy and that MPEs are in fact derived from SAR. Accordingly, the SAR computations provide a scientifically valid and more relevant estimate of human exposure to RF energy. Additional eight simulations have been performed to evaluate SAR for two trunk mount antennas operating at 450 MHz.

Method

The simulation code employed is XFDTD™ v6.4, by Remcom Inc., State College, PA. This computational suite features a heterogeneous full body standing model (High Fidelity Body Mesh), derived from the so-called Visible Human [4], discretized in 5 mm voxels. The dielectric properties of 23 body tissues are automatically assigned by XFDTD™ at any specific frequency. The "seated" man model was obtained from the standing model by modifying the articulation angles at the hips and the knees. Details of the computational method and model are provided in the Appendix to this report.

The car model has been imported into XFDTD™ from the CAD file of a sedan car having dimensions 4.98 m (L) x 1.85 m (W) x 1.18 m (H), and discretized in 5mm voxels. The Figure 1 below show both the CAD model and the photo of the actual car This CAD model has been incorporated into the IEEE 1528.2 draft standard.

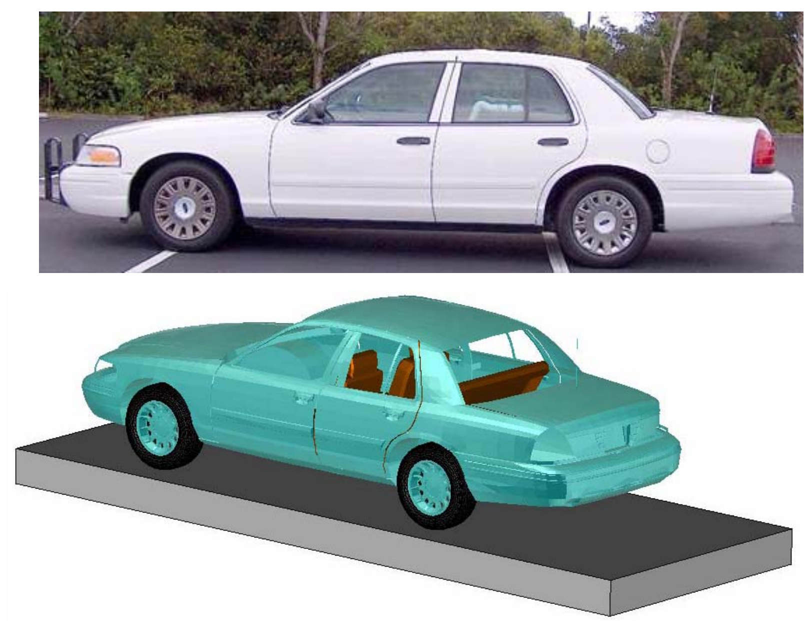

Figure 1: The photo picture of the car used in field measurements and

the corresponding CAD model used in simulations

For bystander exposure, the antenna position is in the center of the trunk, so as to replicate the experimental conditions used in MPE measurements. For passenger exposure, the antenna position is on the trunk and/or in the center of the roof and the distance of trunk mounted antennas from the passenger head when the passenger is located in the center of the back seat was set at 85 cm, also to replicate the experimental conditions used in MPE measurements. Figures 2 and 3 show the XFDTD™ computational models used for bystander exposure. According to the IEEE 1528.2 draft standard (January, 2010) for bystander exposure simulations from vehicle mount antennas the lossy dielectric slab with 30 cm thickness, dielectric constant of 8 and conductivity of 0.01 S/m has been introduced in the computational model to properly account for the effect of the ground (pavement) on exposure. Figure 4 shows some of the XFDTD™ computational models used for passenger exposure to trunk mounted antennas.

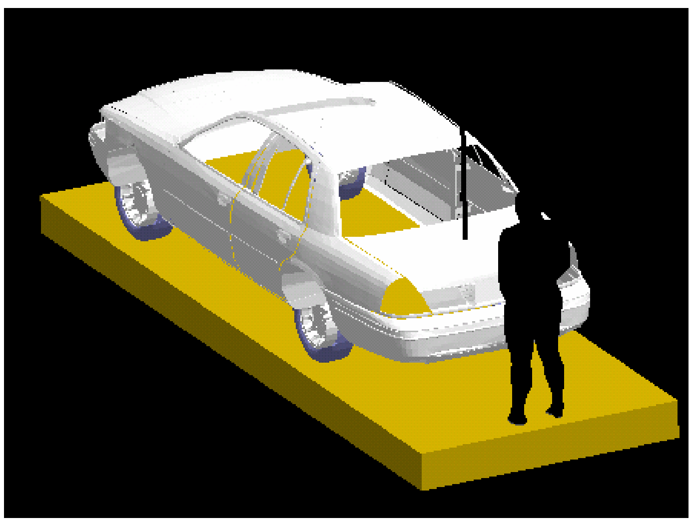

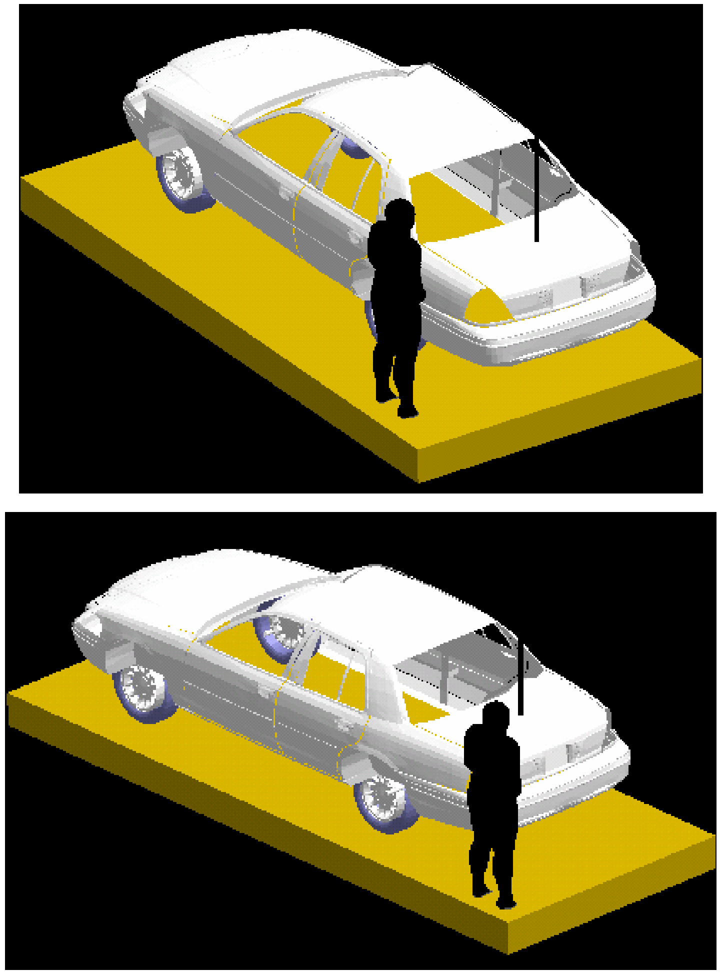

Figure 2: Bystander model exposed to a trunk-mount antenna: Bystander is located at the back, on the side or at the corner of the car replicating the measurement conditions. The antenna is mounted in the center of the trunk. The dielectric slab under the car is introduced to model the ground (pavement) effect on exposure.

Figure 3: Top view of bystander exposure model four different locations relative to the vehicle model that replicate the measurement conditions.

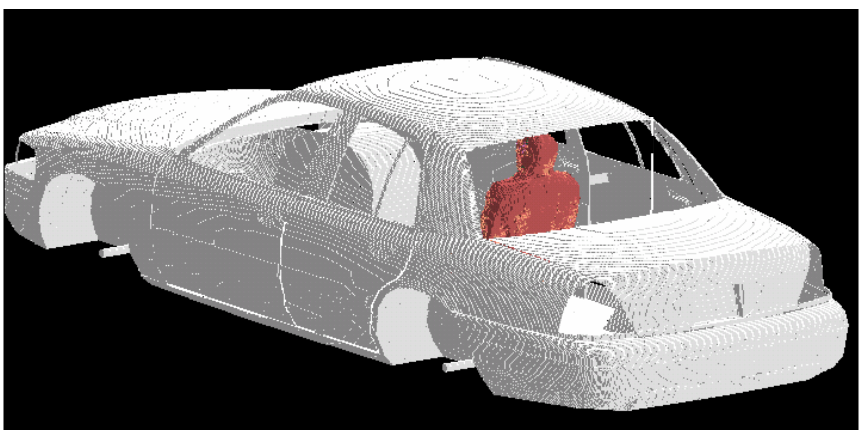

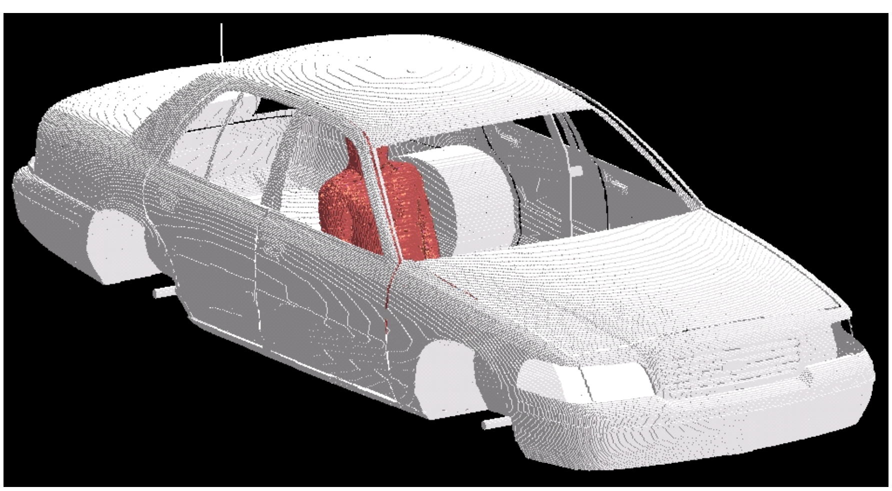

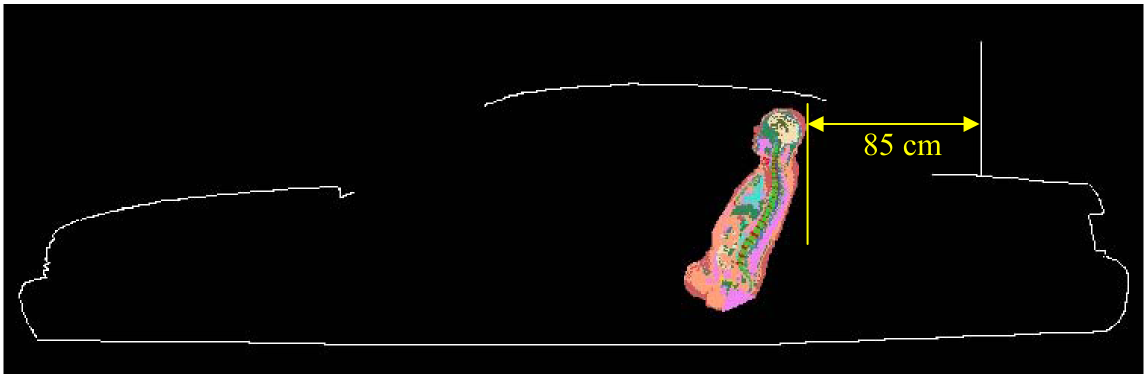

Figure 4: Passenger model exposed to a trunk-mount antenna: XFDTD geometry. The antenna is mounted at 85 cm from the passenger located in the center of the back seat.

The computational code employs a time-harmonic excitation to produce a steady state electromagnetic field in the exposed body. Subsequently, the corresponding SAR distribution is automatically processed in order to determine the whole-body and 1-g average SAR. The maximum average output power from mobile radio antenna is 120 W. Since the ohmic losses in the cable and in the car materials, as well as the mismatch losses at the antenna feed-point, are neglected, and source-based time averaging (50% talk time) is employed, all computational results are normalized to half of it, i.e., 60 W average net output power.

Results of SAR computations for car passengers

The test conditions requiring SAR computations are summarized in Table I, together with the antenna data, the SAR results, and power density (P.D.) percentage of the limit as obtained from the measurements in the corresponding test conditions. The conditions are for antennas mounted on the trunk and on the roof. The antenna length in Table I includes the 1.8 cm magnetic mount base used in measurements to position the antenna on the vehicle. The passenger is located in the center or on the side of the rear seat and in two cases in the front seat. The passenger model is surrounded by air, as the seat, which is made out of poorly conductive fabrics, is not included in the computational model. All the transmit frequency, antenna length, and passenger location combinations reported in Table I have been simulated individually.

Table I: Results of the SAR computations for passenger exposure (50% talk-time).

Mount location	Antenna Kit #	Antenna length with mag. mount base		Freq [MHz]	Max P.D. [mW/cm^2]	Exposure location	SAR [W/kg]	
		Physical	XFDTD				1-g	WB
Trunk	HAE6010A	64.8 cm	65 cm	380	0.53	Center	0.46	0.0251
						Side	0.42	0.0225
				406.5	0.60	Center	0.42	0.0263
						Side	0.47	0.024
				433	0.24	Center	0.46	0.0251
						Side	0.56	0.0215
Trunk	HAE6011A	93.3 cm	95 cm	380	0.34	Center	0.46	0.0135
						Side	0.46	0.0113
				406.5 **Fig. 7**	0.35	Center	0.69	0.0203
						Side	0.58	0.0211
Trunk	HAE4011A	74.5 cm	74.5 cm	450	0.46	Center	0.28	0.0126
						Side	0.26	0.012
				460	0.45	Center	0.25	0.0127
						Side	0.42	0.0143
Trunk	HAE6013A	30.8 cm	31 cm	380	0.76	Center	0.75	0.0296
						Side	0.68	0.0292
				425	0.55	Center	0.38	0.019
						Side	0.52	0.0198
				450 **Fig. 5 & 6**		Center	0.85	0.0382
						Side	0.99	0.0270
				470	0.36	Center	0.58	0.0248
						Side	0.55	0.0289
Trunk	HAE6031A	29.8 cm	30 cm	380	0.81	Center	0.72	0.0292
						Side	0.67	0.0287
				425	0.53	Center	0.46	0.0268
						Side	0.52	0.0267
				450		Center	0.85	0.0384
						Side	0.92	0.0272
				470	0.50	Center	0.54	0.025
						Side	0.54	0.0286
Roof	HAE6012A	20.0 cm	20 cm	406.5 **Fig. 8**	0.26	Center	0.16	0.008
						Side	0.14	0.0086
Roof	HAE6010A	64.8 cm	65 cm	406.5	0.30	Center	0.19	0.009
						Side	0.15	0.0099
Trunk	HAE6013A	30.8 cm	31 cm	380	0.23	Front	0.31	0.0208
Trunk	HAE6031A	29.8 cm	30 cm	380	0.22	Front	0.4	0.0185

The SAR distribution in the passenger model in the exposure condition that gave highest 1-g SAR is reported in Figure 5 (450 MHz, passenger on the side of the back seat, HAE6013A antenna).

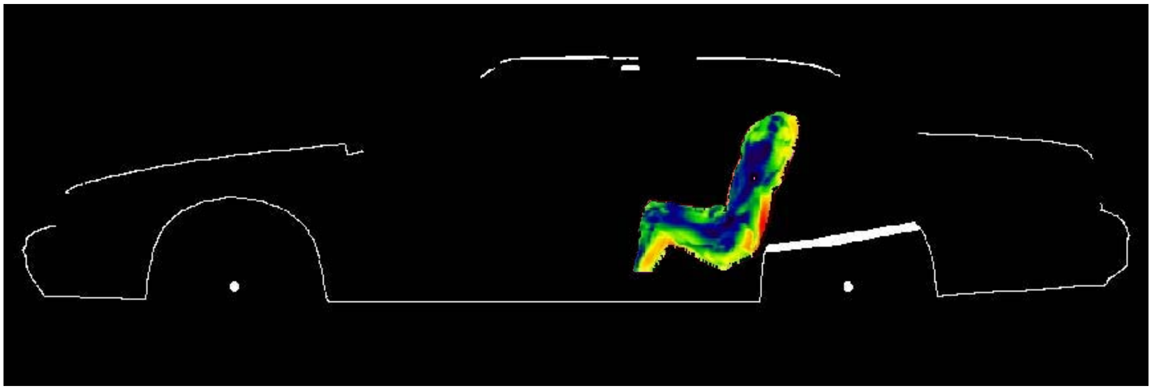

Figure 5. SAR distribution at 450 MHz in the passenger located on the side of the back seat, produced by the trunk-mount HAE6013A antenna. The contour plot in the figure is relative to the plane where the peak 1-g average SAR for this exposure condition occurs.

The two pictures below in Figure 6 show the E and H field distributions in the plane of the antenna corresponding to the condition in Figure 5.

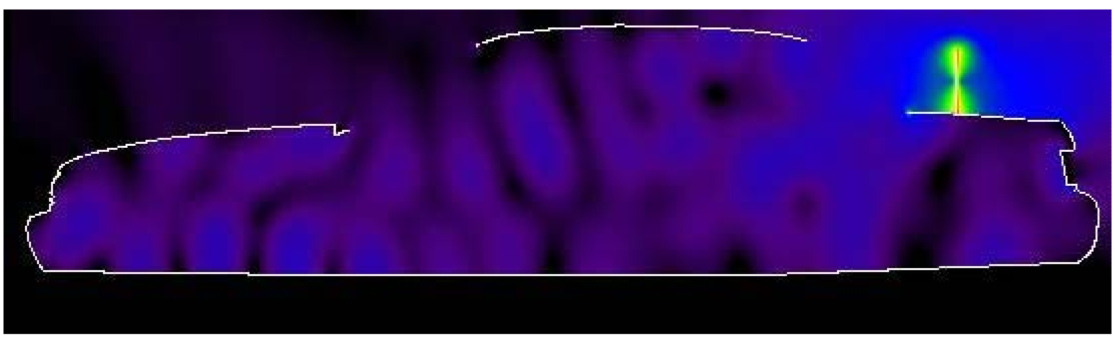

a)

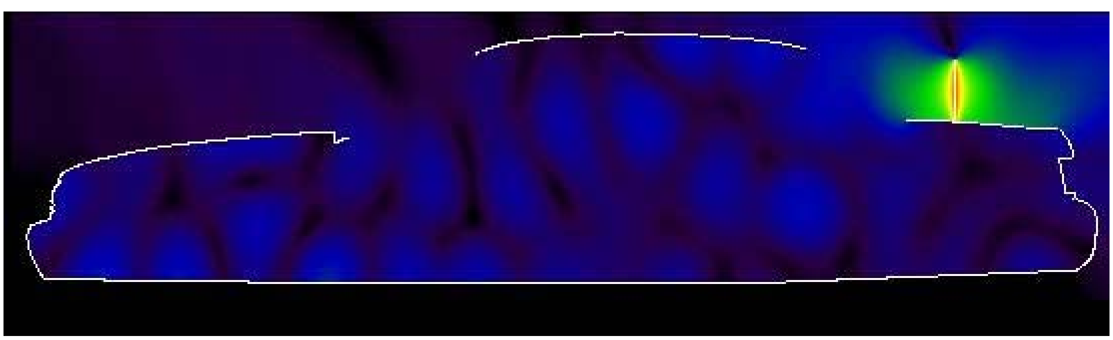

b)

Figure 6. (a) E-field distribution corresponding to exposure condition of Figure 5, and (b) H-field distribution corresponding to exposure condition of Figure 5.

The electric and magnetic field distributions for the passenger exposure configuration and different type of simulated antenna (HAE6011A) relative to the plane where antenna is located are shown in Figure 7.

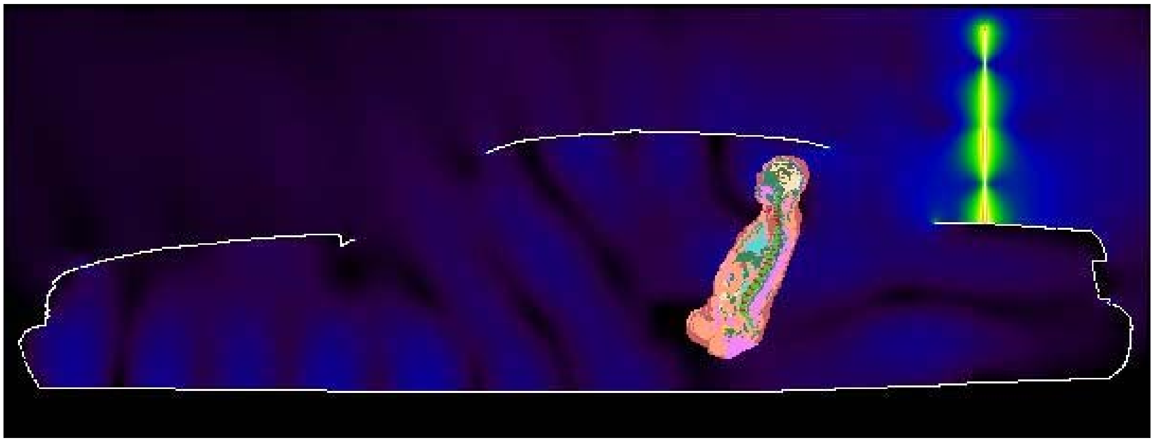

a)

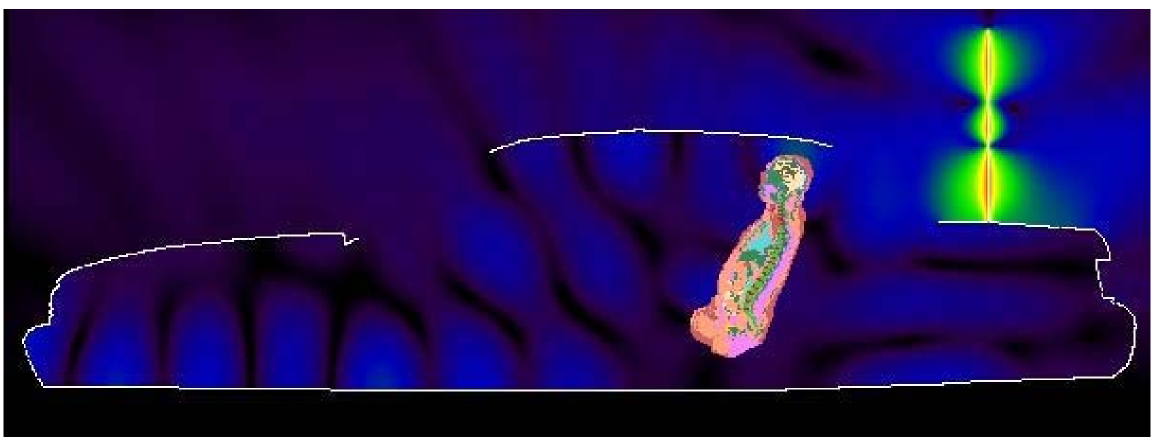

b)

Figure 7. (a) E-field distribution and (b) H-field distribution in the plane of the trunk mounted antenna (HAE6011A antenna at 406.5 MHz) corresponding to the passenger exposure condition

Another example of the E and H field distributions from the HAE6012A roof mount antenna is shown in Figure 8. The distributions are shown relative to the plane where the antenna is located.

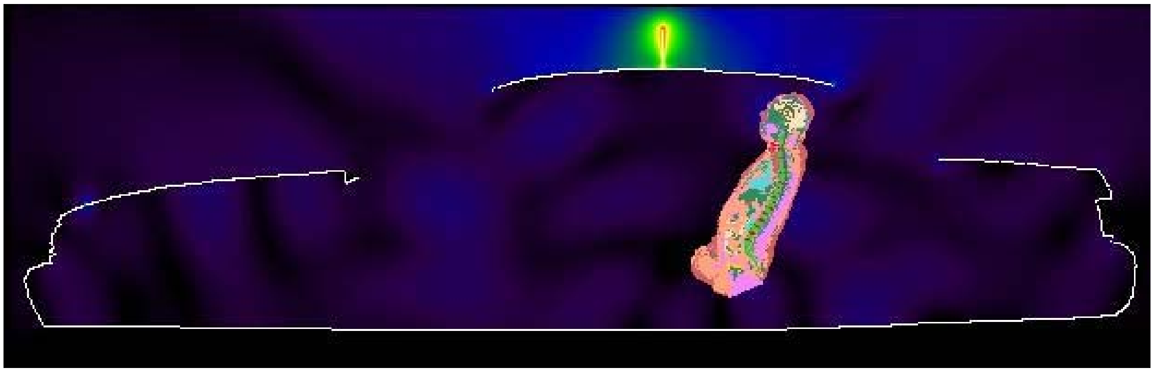

a)

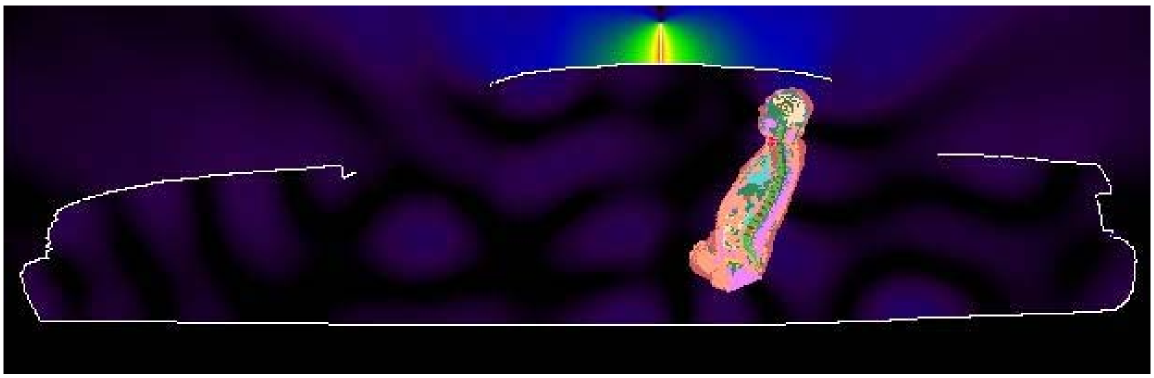

b)

Figure 8. (a) E-field distribution and (b) H-field distribution in the plane of the roof mount antenna (HAE6012A antenna at 406.5 MHz) corresponding to the passenger exposure condition

Results of SAR computations for bystanders

The test conditions requiring SAR computations are summarized in Table II, together with other relevant information and the SAR results. With trunk mount antennas, the bystander is placed at the corner of the trunk, at the back of the trunk or on the side of the trunk as close as possible to the car while maintaining at least 90 cm separation from the antenna and 20 cm separation from the car. Two cases of bystander - facing towards or away from the car - were simulated individually.

Table II: Results of the SAR computations for bystander exposure (50% talk-time). The bystander is placed at the corner of the trunk (45 deg), at the back of the trunk or on the side of the trunk (90 deg) as close as possible to the car while maintaining at least 90 cm separation from the antenna and 20 cm separation from the car

Mount location	Antenna Kit #	Antenna length		Freq [MHz]	Max P.D. [mW/cm^2]	Exposure location	SAR [W/kg]	
		Physical	XFDTD				1-g	WB
Trunk	HAE6010A	64.8 cm	65 cm	380	0.22	Front	0.45	0.0172
						Back	0.38	0.0193
				406.5	0.29	Front	0.56	0.0172
						Back	0.45	0.0196
Trunk	HAE6011A	93.3 cm	93.5 cm	380 **Fig. 9 & 10**	0.23	Front	0.9	0.0189
						Back	0.63	0.0229
Trunk	HAE6013A	30.8 cm	31 cm	380 **Fig. 11**	0.33	Front	0.57	0.0233
						Back	0.6	0.0284
				425	0.34	Front	0.53	0.0205
						Back	0.42	0.0238
				450		Front	0.30	0.0112
						Back	0.29	0.0124
Trunk	HAE6031A	29.8 cm	30 cm	380	0.29	Front	0.55	0.0233
						Back	0.59	0.0279
				425	0.36	Front	0.53	0.0205
						Back	0.41	0.0238
				450		Front	0.30	0.0113
						Back	0.29	0.0125
				470	0.30	Front	0.66	0.0197
						Back	0.52	0.0206
				425 **Fig. 12**	0.26	Front, 45 deg	0.48	0.018
						Back, 45 deg	0.56	0.0171
				425	0.29	Front, 90 deg	0.51	0.0148
						Back, 90 deg	0.52	0.0187

The SAR distribution in the bystander model in the exposure condition that gave highest 1-g SAR is reported in Figure 9 (380 MHz, bystander at the back of the trunk facing the car, HAE6011A antenna).

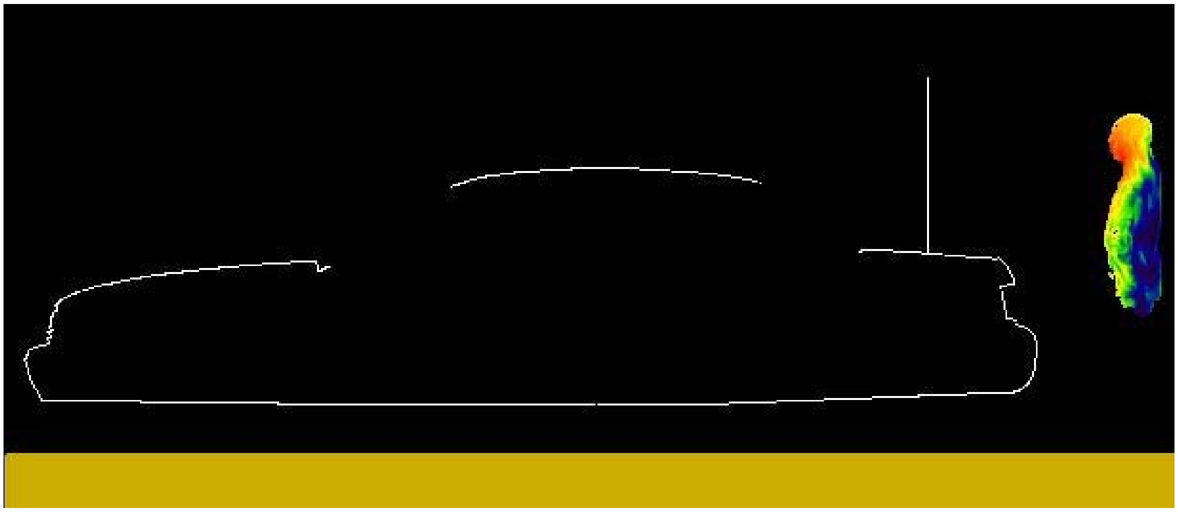

Figure 9. SAR distribution at 380 MHz in the bystander located at back of the trunk, produced by the trunk-mount HAE6011A antenna. The contour plot for SAR distribution in the figure is relative to the plane where the peak 1-g average SAR for this exposure condition occurs.

The two pictures below show the E and H field distributions in the plane of the antenna corresponding to the condition represented in Figure 9.

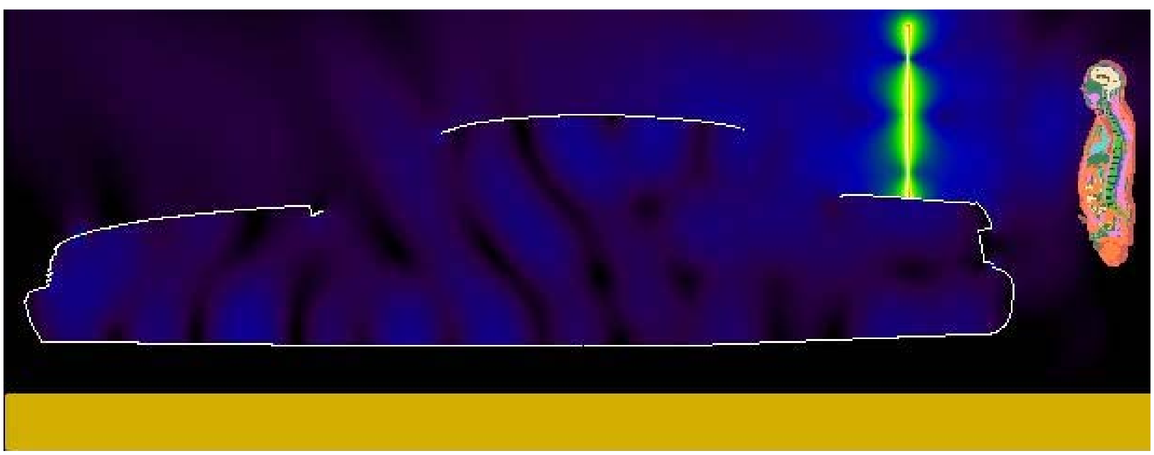

a)

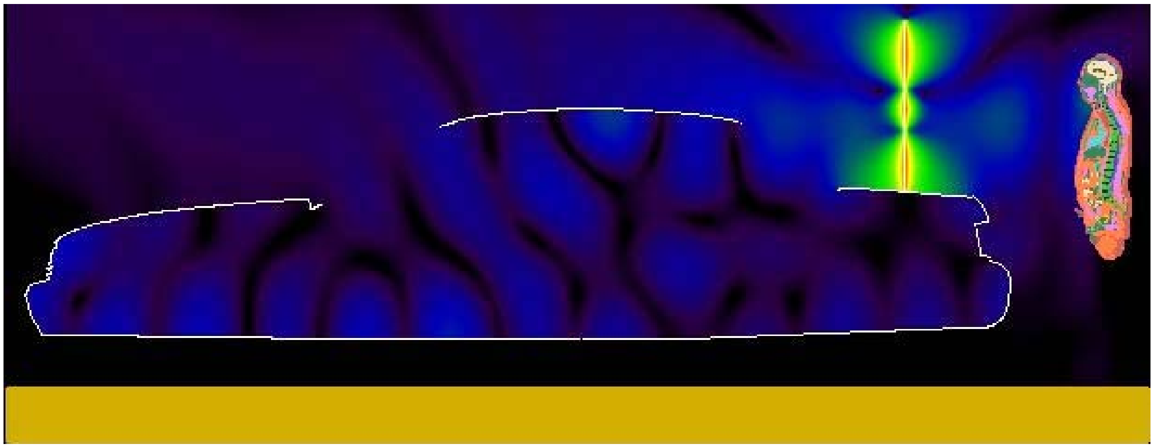

b)

Figure 10. (a) E-field distribution in the plane of the antenna corresponding to exposure condition of Figure 8, and (b) H-field distribution corresponding to exposure condition of Figure 9.

Another example of the E and H field distributions from the trunk mounted antenna (HAE6013A) in the condition of the bystander exposure that produced highest whole body average SAR (380 MHz, bystander located at the back of the trunk facing away from the car) is shown in Figure 11.

a)

b)

Figure 11. (a) E-field distribution and (b) H-field distribution in the plane of the antenna corresponding to the bystander exposure condition located at the back of the car (HAE6013A antenna at 380 MHz)

Finally, as another example, the E and H field distributions for the trunk mount antenna (HAE6031A) in the condition of the bystander facing the car and located on the side of the trunk is shown in Figure 12.

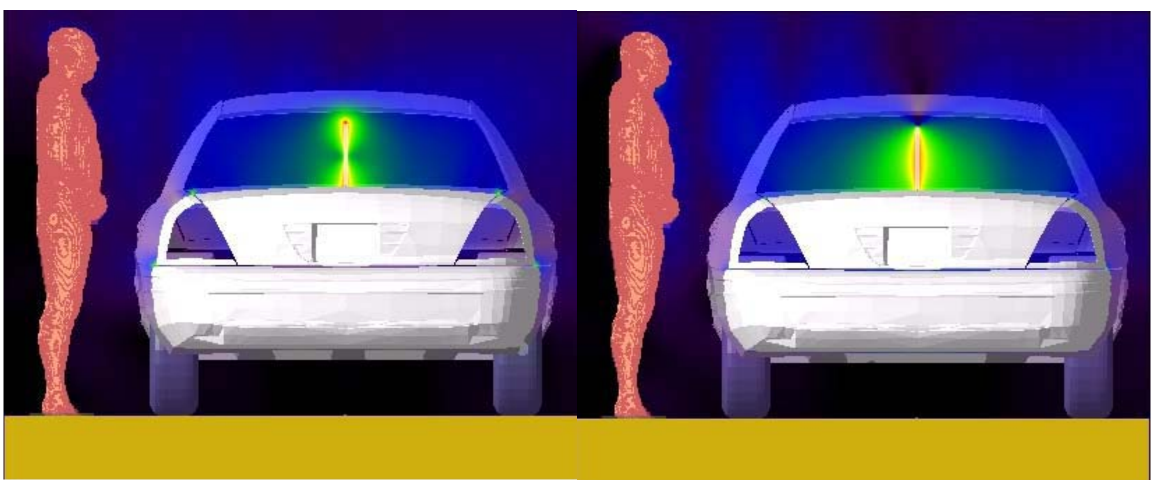

a) b)

Figure 12. (a) E-field distribution and (b) H-field distribution in the plane of the antenna corresponding to the bystander exposure condition located at the side the trunk (HAE6031A antenna at 425 MHz)

The overall maximum peak 1-g SAR in all simulated conditions is 0.99 W/kg, less than the 1.6 W/kg limit, while the maximum whole-body average SAR is 0.0384 W/kg, less than the 0.08 W/kg limit.

Conclusions

Under the test conditions described for evaluating passenger and bystander exposure to the RF electromagnetic fields emitted by vehicle-mounted antennas used in conjunction with this mobile radio product, the present analysis shows that the computed SAR values are compliant with the FCC exposure limits for the general public.

In addition to the above results the highest SAR configurations for passenger and bystander were simulated again using the newer version 7.1 of the XFDTD™ code, by Remcom Inc., featuring adaptive mesh and higher, 3-mm resolution human body model.

Mount location	Position	Antenna	Freq. (MHz)	SAR (mW/g)	
				XFDTD, V6.4	XFDTD, V7.1
Trunk	Passenger	HAE6013A	450	0.99	0.76
Trunk	Bystander	HAE6011A	380	0.90	0.86

References

[1] IEEE Standard C95.1-1999. *IEEE Standard for Safety Levels with Respect to Human Exposure to RF Electromagnetic Fields*, 3 kHz to 300 GHz.

[2] http://www.nlm.nih.gov/research/visible/visible_human.html

APPENDIX: SPECIFIC INFORMATION FOR SAR COMPUTATIONS

This appendix follows the structure outlined in Appendix B.III of the Supplement C to the FCC OET Bulletin 65. Most of the information regarding the code employed to perform the numerical computations has been adapted from the draft IEEE 1528.1 and 1528.2 standards, and from the XFDTD™ v5.3 and v6.4. User Manuals. Remcom Inc., owner of XFDTD™, is kindly acknowledged for the help provided.

1) Computational resources

a) A multiprocessor system equipped with two Intel Xeon X5570 quad-core CPUs was employed for all simulations.

b) The memory requirement was from 7 GB to 10 GB. Using the above-mentioned system with 8-cores operating concurrently, the typical simulation would run for 3-5 hours.

2) FDTD algorithm implementation and validation

a) We employed a commercial code (XFDTD™ v6.4, by Remcom Inc.) that implements the Yee's FDTD formulation [1]. The solution domain was discretized according to a rectangular grid with a uniform 5 mm step in all directions. Sub-gridding was not used. Liao's absorbing boundary conditions [2] are set at the domain boundary to simulate free space radiation processes. The excitation is a lumped voltage generator with 50-ohm source impedance. The code allows selecting *wire objects* without specifying their radius. We used a wire to represent the antenna. The car body is modeled by solid metal. We did not employ the "thin wire" algorithm in XFDTD™ since the antenna radius was never smaller than one-fifth the voxel dimension. In fact, the XFDTD™ manual specifies that "Thin Wire materials may be used in special situations where a wire with a radius much smaller than the cell size is required… in cases where the wire radius is important to the calculation and is less than approximately 1/5 the cell size, the thin wire material may be used to accurately simulate the correct wire dimensions." The voxel size in all our simulations was 5 mm, and the antenna radius is always at least 1 mm (1 mm for the short quarter-wave antennas and 1.5 mm for the long gain antennas), so there was no need to specify a "thin wire" material. Because the field impinges on the bystander or passenger model at a distance of several tens of voxels from the antenna, the details of antenna wire modeling are not expected to have significant impact on the exposure level.

Some antennas have inductive loading coils located in the mid section as shown in the picture below of the HAE 6010A or HAE 6011A antenna examples.

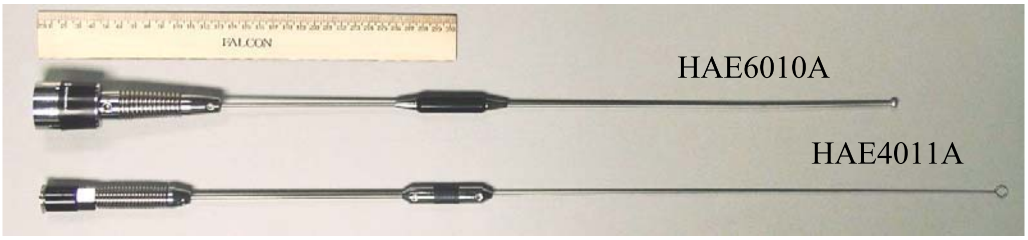

The X-ray of the reactive loads of the HAE4011A and HAE6010A antennas is also presented in the next pictures below. Those elements are significantly shorter than the length of the antenna and are about 1/40 of the wavelength at center operating frequency. They were modeled as lumped reactive elements. The comparison with measurements and validity of such simulation model has been summarized in [9].

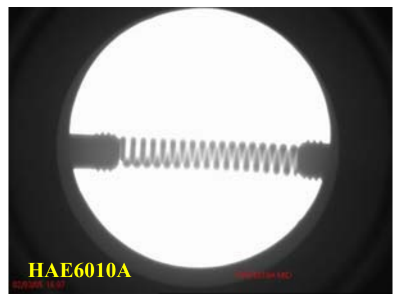

b) XFDTD™ is one of the most widely employed commercial codes for electromagnetic simulations. It has gone through extensive validation and has proven its accuracy over time in many different applications. One example is provided in [3].

We carried out a validation of the code algorithm by running the canonical test case involving a half-wave wire dipole. The dipole is 0.475 times the free space wavelength at 400 MHz, i.e., about 35.5 cm long. The discretization used in the model was uniform in all directions and equal to 5 mm, so the dipole was 71 cells long. Also in this case, the "thin wire" model was not needed. The following picture shows XFDTD™ outputs regarding the antenna feed-point impedance (75.20 + j 11.8 ohm), as well as qualitative distributions of the total E and H fields near the dipole. The radiation pattern is shown as well (one lobe in elevation). As expected, the 3 dB beamwidth is about 78 degrees.

Complex Feed Point Impedance (Ohms)

Feed	Real	Imaginary	
1	75.253304	11.832200	

The computed results are in good agreement with the known analytical results for the half -wave dipole antenna which could be found in [10].

This validation ensures that the input impedance calculation is carried out correctly in XFDTD™, thereby enabling accurate estimates of the radiated power. It further ensures that the wire model employed in XFDTD™, which we used to model the antennas, produces physically meaningful current and fields distributions. Both these aspects ensure that the field quantities are correctly computed both in terms of absolute amplitude and relative distribution.

3) Computational parameters

a) The following table reports the main parameters of the FDTD model employed to

Total E-field **Total H-field**

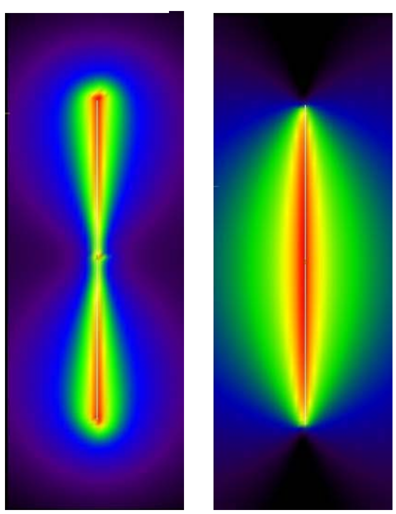

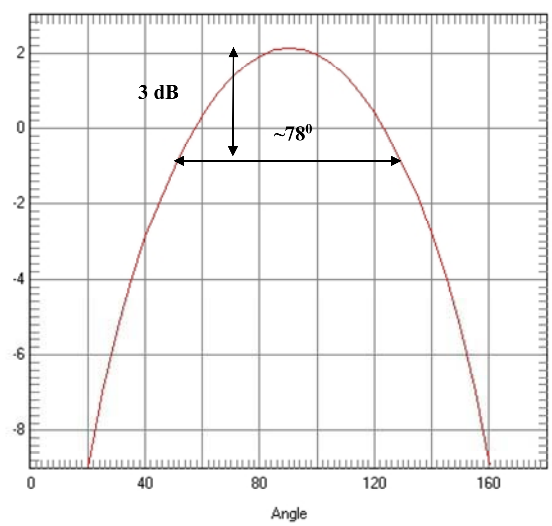

perform our computational analysis:

PARAMETER	X	Y	Z
Voxel size	5 mm	5 mm	5 mm
Maximum domain dimensions employed for passenger computations with the trunk-mount antennas	425	1104	289
Maximum domain dimensions employed for bystander computations with the trunk-mount antennas	434	1243	580
Time step	Exactly equal to Courant limit (typically 10 *ps* at this frequency, with the body model)		
Objects separation from FDTD boundary (voxels)	>10	>10	>10
Number of time steps for passenger	Enough to reach at least -40 dB convergence		
Excitation	Sinusoidal (not less than 10 periods)		

4) Phantom model implementation and validation

a) The FDTD mesh of a male human body was created using digitized data in the form of transverse color images. The data is from the *visible human project* sponsored by the National Library of Medicine (NLM) and is available via the Internet (http://www.nlm.nih.gov/research/visible/visible_human.html). The male data set consists of MRI, CT and anatomical images. Axial MRI images of the head and neck and longitudinal sections of the rest of the body are available at 4 mm intervals. The MRI images have 256 pixel by 256 pixel resolution. Each pixel has 12 bits of gray tone resolution. The CT data consists of axial CT scans of the entire body taken at 1 mm intervals at a resolution of 512 pixels by 512 pixels where each pixel is made up of 12 bits of gray tone. The axial anatomical images are 2048 pixels by 1216 pixels where each pixel is defined by 24 bits of color. The anatomical cross sections are also at 1 mm intervals and coincide with the CT axial images. There are 1871 cross sections. The XFDTD™ High Fidelity Body Mesh uses 5x5x5 mm cells and has dimensions 136 x 87 x 397. Dr. Michael Smith and Dr. Chris Collins of the Milton S. Hershey Medical Center, Hershey, Pa, created the High Fidelity Body mesh. Details of body model creation are given in the *methods* section in [5]. The body mesh contains 23 tissues materials. Measured values for the tissue parameters for a broad frequency range are included with the mesh data. The correct values are interpolated from the table of measured data and entered into the appropriate mesh variables. The tissue conductivity and permittivity variation *vs.* frequency is included in the XFDTD™ calculation by a multiple-pole approximation to the Cole-Cole approximated tissue parameters reported by Camelia Gabriel, Ph.D., and Sami Gabriel, M. Sc. (http://www.brooks.af.mil/AFRL/HED/hedr/reports/dielectric/home.html).

a) The XFDTD™ High Fidelity Body Mesh model correctly represents the anatomical structure and the dielectric properties of body tissues, so it is appropriate for determining the highest exposure expected for normal device operation.

b) One example of the accuracy of XFDTD™ for computing SAR has been provided in [6]. The study reported in [6] is relative to a large-scale benchmark of measurement and computational tools carried out within the IEEE Standards Coordinating Committee 34, Sub-Committee 2.

5) Tissue dielectric parameters

a) The following table reports the dielectric properties used by XFDTD™ for the 23 body tissue materials in the High Fidelity Body Mesh at 450 MHz.

#	Tissue	ε_r	σ (S/m)	Density (kg/m^3)
1	skin	41.5	0.57	1125
2	tendon, pancreas, prostate, aorta, liver, other	50.3	0.76	1151
3	fat, yellow marrow	5.02	0.05	943

4	cortical bone	13.4	0.11	1850
5	cancellous bone	21.0	0.23	1080
6	blood	57.2	1.72	1057
7	muscle, heart, spleen, colon, tongue	63.5	0.99	1059
8	gray matter, cerebellum	54.1	0.88	1035.5
9	white matter	39.7	0.54	1027.4
10	CSF	68.9	2.32	1000
11	sclera/cornea	54.4	1.04	1151
12	vitreous humor	68.3	1.56	1000
13	bladder	17.6	0.31	1132
14	nerve	35.5	0.50	1112
15	cartilage	43.4	0.66	1171
16	gall bladder bile	76.5	1.62	928
17	thyroid	59.8	0.82	1035.5
18	stomach/esophagus	74.4	1.13	1126
19	lung	52.8	0.72	563
20	kidney	57.0	1.16	1147
21	testis	65.2	1.13	1158
22	lens	51.9	0.71	1163
23	small intestine	73.7	2.07	1153

b) The tissue types and dielectric parameters used in the SAR computation are appropriate for determining the highest exposure expected for normal device operation, because they are derived from measurements performed on real biological tissues (http://www.brooks.af.mil/AFRL/HED/hedr/reports/dielectric/home.html).

c) The tabulated list of the dielectric parameters used in phantom models is provided at point 5(a). As regards the device (car plus antenna), we used perfect electric conductors.

6) Transmitter model implementation and validation

a) The essential features that must be modeled correctly for the particular test device model to be valid are:

- Car body. We developed one very similar to the car used for MPE measurements, so as to be able to correlate measured and simulated field values. The model was imported in XFDTD™ from a CAD model that is commercially available at http://www.3dcadbrowser.com/
- Antenna. We used a straight wire, even when the gain antenna has a base coil for tuning. All the coil does is compensating for excess capacitance due to the antenna being slightly longer than half a wavelength. We do not need to do that in the model, as we used normalization with respect to the net radiated power, which is determined by the input resistance only. In this way, we neglect mismatch losses and artificially produce an overestimation of the SAR, thereby introducing

a conservative bias in the model. In case of low profile vertical monopole antenna (HAE6016A) which has an additional horizontal metal circular disk at the tip, the disk was included in the model and well represented in 5 mm resolution mesh.

- Antenna location. We used the same location, relative to the edge of the car trunk, the backseat, or the roof, used in the MPE measurements. The following pictures show a lateral and a perspective view of the whole model (XFDTD™ does not show wires in this type of view, that is why the antenna is not visible).

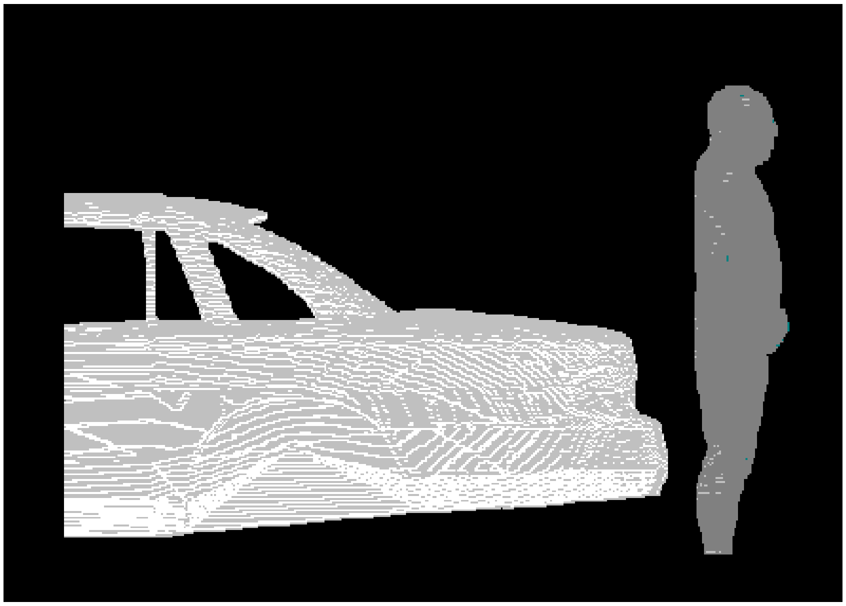

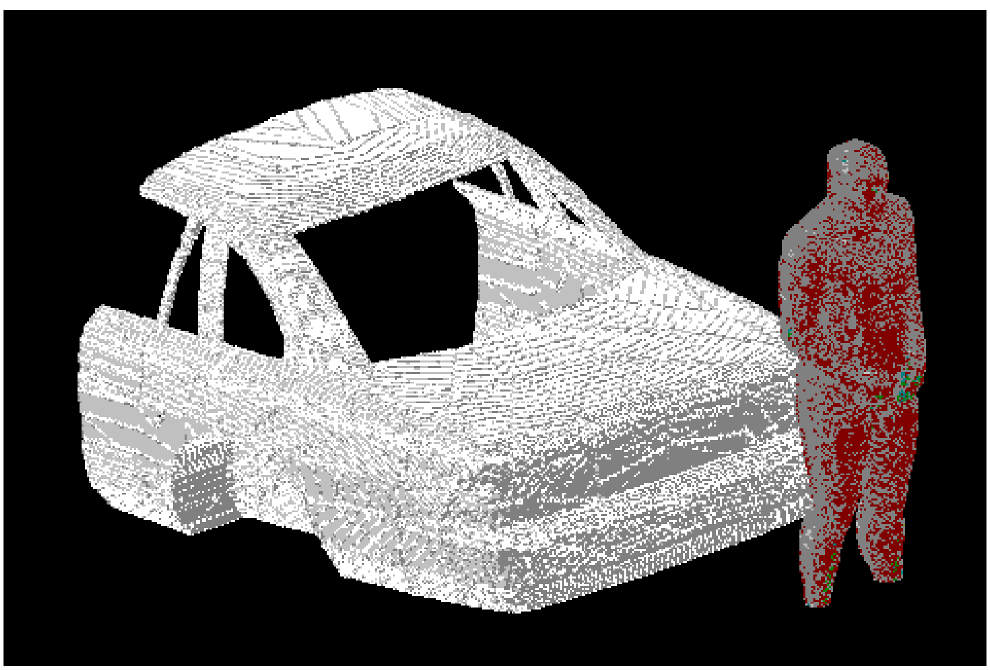

The car model is constituted by perfect electric conductor and does not include wheels in order to reduce its complexity. The passenger model is surrounded by air, as the seat, which is made out of poorly conductive fabrics, is not included in the computational model. The passenger and bystander models were validated for similar antenna and frequency conditions by comparing the MPE measurements at UHF frequencies (421.5 MHz and 425 MHz) for similar antennas used for a UHF mobile radio. The comparison results are presented below, according to following definitions for the equivalent power densities (based on E or H-field):

$$S_E = \frac{|\mathbf{E}|^2}{2\eta}, \quad S_H = \frac{\eta}{2}|\mathbf{H}|^2, \quad \eta = 377\,\Omega$$

<u>Passenger with 17.5 cm monopole antenna (HAE4002A 421.5 MHz)</u>

The following figure of the test model shows the car model, where the yellow dots individuate the back seat, as it can be observed from the other figure showing the cross section of the passenger. The comparison has been performed by taking the average of the computed steady-state field values at the six dotted locations, corresponding to the head, chest, and legs along the yellow dots line, and comparing them with the average of the MPE measurements performed at the head, chest and legs locations. Such a comparison is carried out at the same average power level (22 W, including the 50% duty factor) used in the MPE measurements.

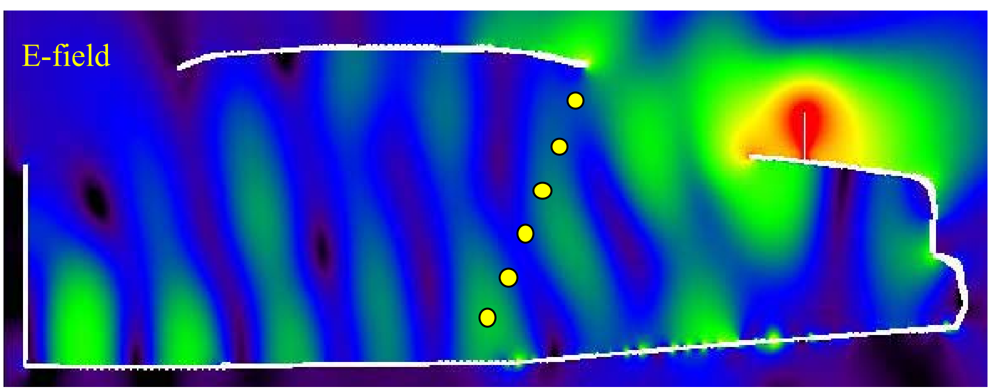

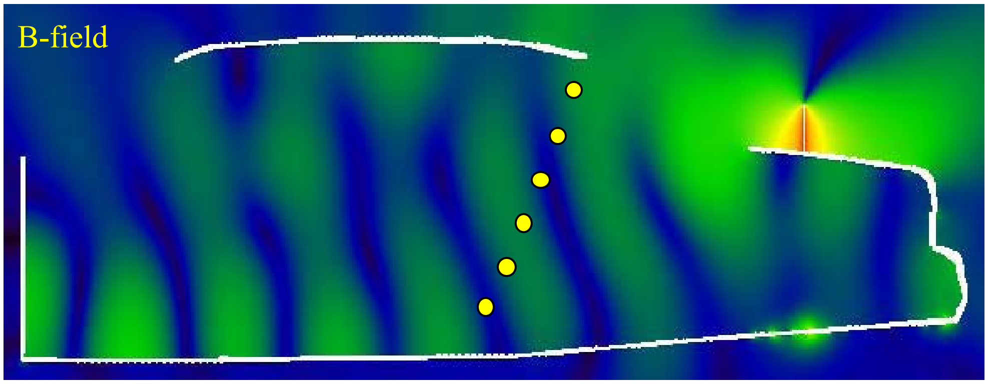

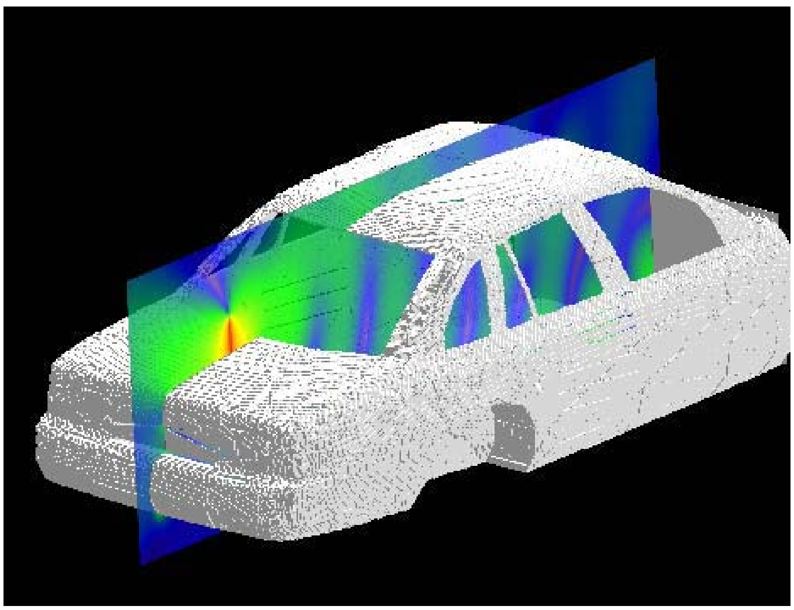

The equivalent power density (S) is computed from the E-field and the H-field separately. The following table reports the E-field values computed by XFDTD™ at the six locations, and the corresponding power density.

Location Number	E-field, V/m	Eq. Power Density 1.0 V source	Scaled Power Dens. 22 W output, mW/cm^2
1	5.83E-01	4.51E-04	4.41E-01
2	6.31E-01	5.28E-04	5.16E-01
3	6.50E-01	5.60E-04	5.48E-01
4	5.50E-01	4.01E-04	3.92E-01
5	4.50E-01	2.69E-04	2.63E-01
6	7.80E-01	8.07E-04	7.89E-01
Equivalent average Power Density			**4.92E-01**

Location Number	B-field, Weber/m2	Eq. Power Density 1.0 V source	Scaled Power Dens. 22 W output, mW/cm^2
1	2.26E-09	0.00061	5.96E-01
2	9.00E-10	0.00010	9.45E-02
3	1.20E-09	0.00017	1.68E-01
4	2.20E-09	0.00058	5.65E-01
5	1.90E-09	0.00043	4.21E-01
6	9.00E-10	0.00010	9.45E-02
Equivalent average Power Density			**3.23E-01**

The input impedance is 36.2+j24.8 ohm, therefore the radiated power (considering the mismatch to the 50 ohm unitary voltage source) is 2.25E-3 W, therefore a factor equal to 9779 is required to scale up to 22 W radiated. The corresponding scaled-up power densities are reported in the tables above, which show that the simulation overestimates the average power density from the MPE measurements (0.29 mW/cm^2), as derived from the measured E-field reported in the following table:

Position	**SE (meas), 22 W output mW/cm^2**
Head	0.38
Chest	0.33
Lower Trunk	0.16

The simulations tend to overestimate the average power density levels, which is understandable since there are no ohmic losses and perfect impedance matching is enforced in the computational models. Based on these results, we conclude that the simulation will produce slight exposure overestimates (about12%).

b) Descriptions and illustrations showing the correspondence between the modeled test device and the actual device, with respect to shape, size, dimensions and near-field radiating characteristics, are found in the main report.

c) Verification that the test device model is equivalent to the actual device for predicting the SAR distributions descends from the fact that the car and antenna size and location in the numerical model correspond to those used in the measurements.

d) The peak SAR is in the neck region for the passenger, which is in line with MPE measurements and predictions.

<u>Passenger with 63.5 cm monopole antenna (HAE6010A 425 MHz)</u>

The following figures show the car model with the field distribution in the horizontal planes where the MPE measurements have been performed. The comparison has been performed by taking the average of the computed steady-state field values at the three locations, corresponding to the head, chest, and lower trunk, and comparing them with the average of the MPE measurements performed at the head, chest and lower trunk locations. Such a comparison is carried out at the same average power level (61.5 W, including the 50% duty factor) used in the MPE measurements.

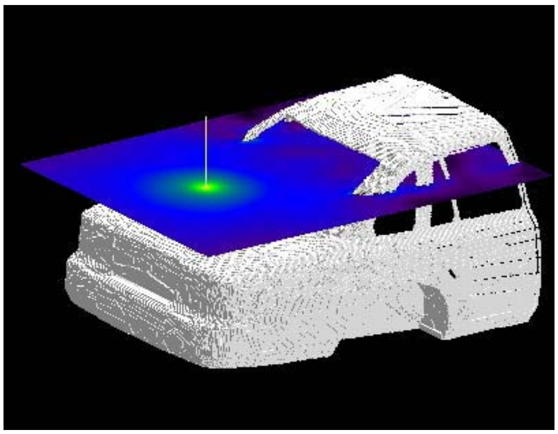

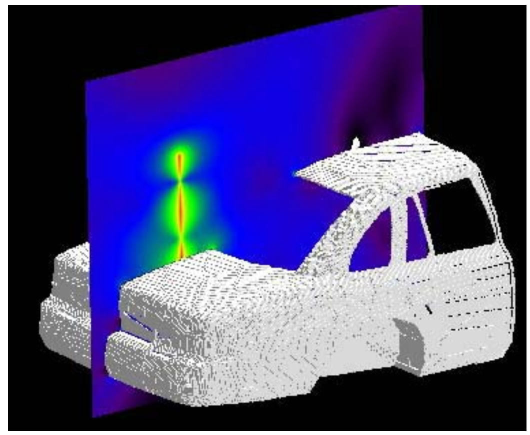

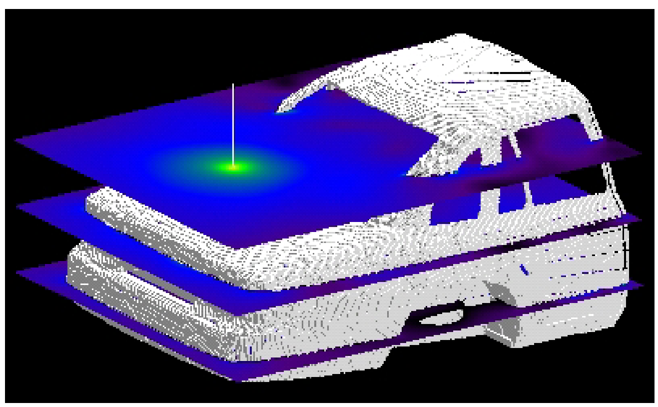

The equivalent power density (S) is computed from the E-field. The following table reports the E-field values computed by XFDTD™ at the three locations, and the corresponding power density.

Location Number	E-field, V/m	Eq. Power Density 1.0 V source	Scaled Power Dens. 61.5 W output, mW/cm^2
1	2.10E-01	5.85E-05	0.561
2	3.66E-01	1.78E-04	1.70
3	1.72E-01	3.92E-04	0.376
Equivalent average Power Density			**0.88**

The corresponding scaled-up power densities are reported in the tables above, which show that the simulation overestimates the average power density from the MPE measurements (0.52 mW/cm^2), as derived from the measured E-field reported in the following table:

Position	SE (meas), 60 W output mW/cm^2
Head	0.72
Chest	0.64
Lower Trunk	0.19

The simulations tend to overestimate the average power density levels, which is understandable since there are no ohmic losses and perfect impedance matching is enforced in the computational models. Based on these results, we conclude that the simulation will produce exposure overestimates (about 69%).

Bystander with 29 cm monopole antenna (HAE6013A 425 MHz)

The following figures show the E-field and H-field distributions across a vertical plane passing for the antenna and cutting the car in half. As done in the measurements, the MPE is computed from both E-field and H-field distributions, along the yellow dotted line at 10 points spaced 20 cm apart from each other up to 2 m in height. These lines and the field evaluation points are approximately indicated in the figures. The E-field and H-field distributions in the vertical plane placed at 90 cm from the antenna, behind the case, are shown as well. The points where the fields are sampled to determine the equivalent power density (S) are approximately indicated by the white dots. A picture of the antenna is not reported because it is identical to the HAE6013A.

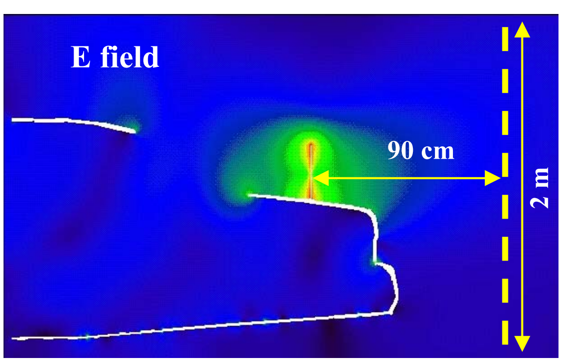

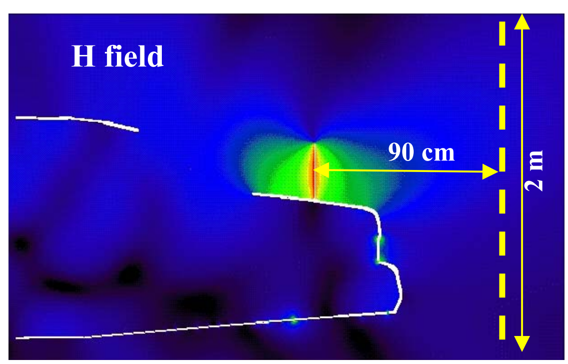

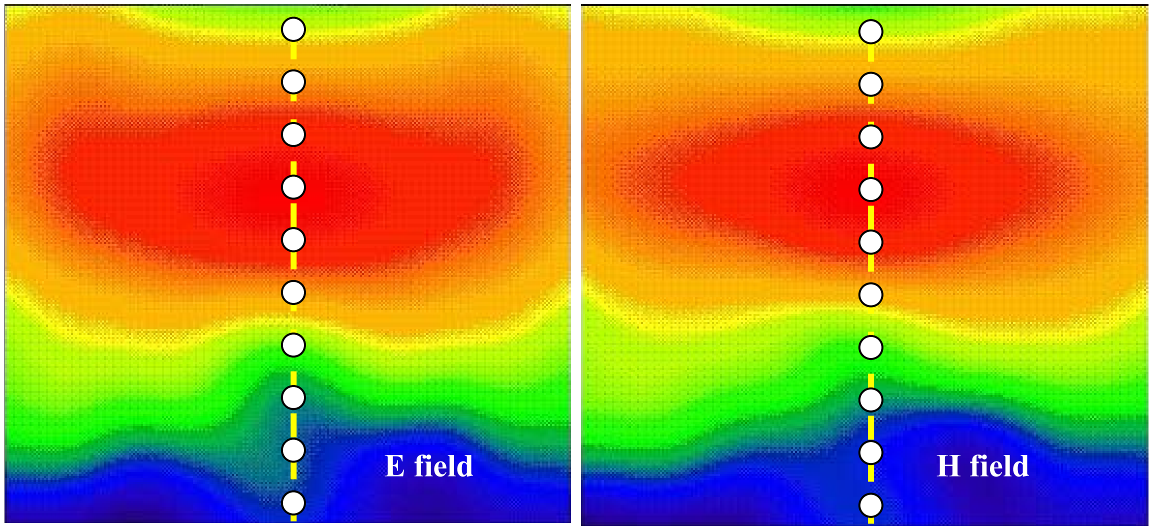

The following table reports the field values computed by XFDTD™ and the corresponding power density values. The average exposure levels are computed as well.

Height (cm)	E (V/m)	S_E (W/m^2)	H (A/m)	S_H (W/m^2)
0	1.05E-01	1.46E-05	2.90E-05	1.589E-05
20	1.14E-01	1.72E-05	2.90E-05	1.598E-05
40	1.16E-01	1.78E-05	3.14E-05	1.871E-05
60	1.39E-01	2.56E-05	3.75E-05	2.669E-05
80	2.03E-01	5.47E-05	5.03E-05	4.795E-05
100	2.73E-01	9.88E-05	7.23E-05	9.923E-05
120	2.94E-01	1.15E-04	8.17E-05	1.266E-04
140	2.65E-01	9.31E-05	7.32E-05	1.016E-04
160	2.12E-01	5.96E-05	5.73E-05	6.219E-05
180	1.60E-01	3.40E-05	4.32E-05	3.531E-05
Average S_E		**5.302E-05**	**Average S_H**	**5.501E-05**

Since the conducted power during the MPE measurement was 123 W the calculated power density was then scaled up for 61.5 W radiated power (taking into account 50% talk time). This model does not include the mismatch loss, loss in the cable and finite conductivity of the car surface and as represents a conservative model for exposure assessment. The scaled-up power density values for 61.5 W radiated power are 5.67 W/m^2 (E), and 5.88 W/m^2 (H), that correspond to 0.57 mW/cm^2 (E), and 0.59 mW/cm^2 (H). Measurements yielded average power density of 0.309 mW/cm^2 (E), which shows that the calculated power density is overestimated. The following graph shows a comparison between the measured power density and the simulated one, based on E or H fields, normalized to 61.5 W radiated power.

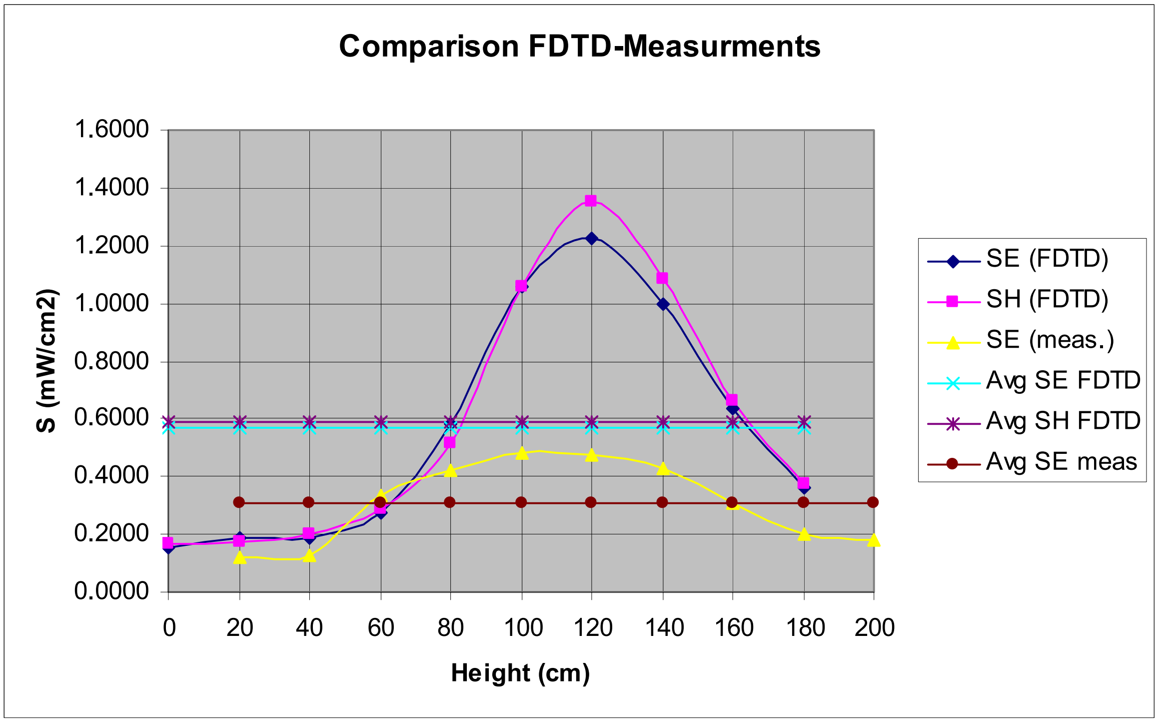

Bystander with 63.5 cm monopole antenna (HAE6010A 425 MHz)

The following figures show the E-field and H-field distributions across a vertical plane passing for the antenna and cutting the car in half. As done in the measurements, the MPE is computed from both E-field and H-field distributions, along the yellow dotted line at 10 points spaced 20 cm apart from each other up to 2 m in height. These lines and the field evaluation points are approximately indicated in the figures. The E-field and H-field distributions in the vertical plane placed at 90 cm from the antenna, behind the case, are shown as well. The points where the fields are sampled to determine the equivalent power density (S) are approximately indicated by the white dots. A picture of the antenna is not reported because it is identical to the HAE6010A.

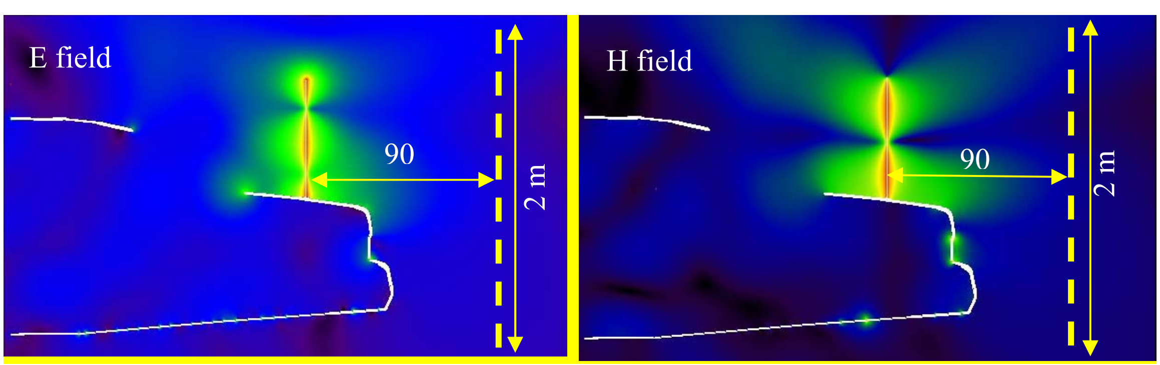

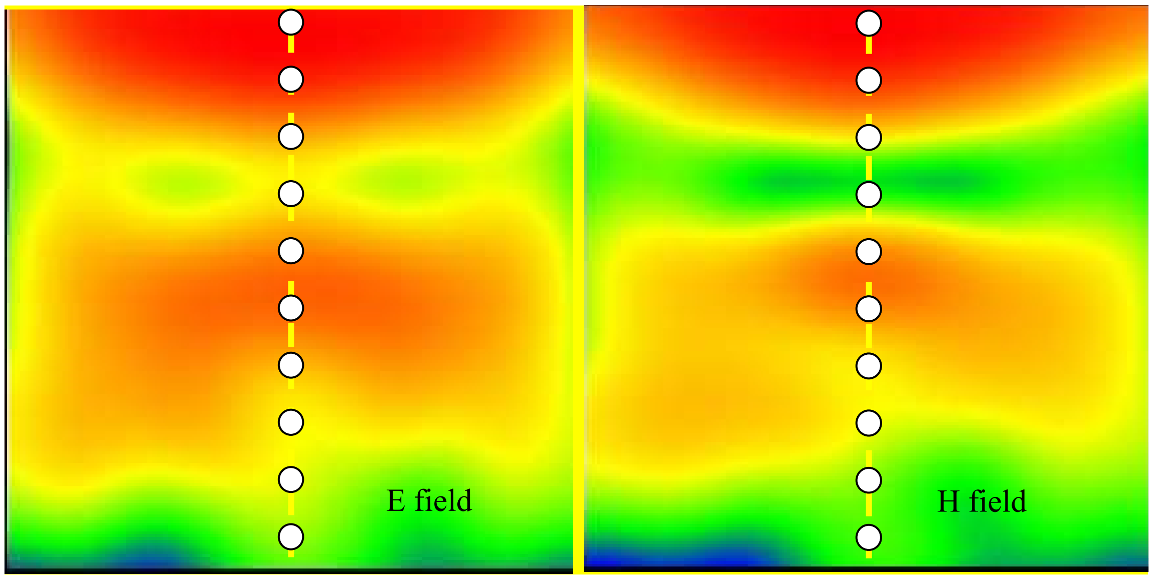

The following table reports the field values computed by XFDTD™ and the corresponding power density values. The average exposure levels are computed as well.

Height (cm)	E (V/m)	S_E (W/m^2)	H (A/m)	S_H (W/m^2)
0	1.32E-01	2.31E-05	4.51E-10	2.43E-05
20	1.49E-01	2.94E-05	4.82E-10	2.77E-05
40	1.58E-01	3.31E-05	5.44E-10	3.53E-05
60	1.71E-01	3.88E-05	5.79E-10	4.00E-05
80	2.10E-01	5.85E-05	6.78E-10	5.48E-05
100	2.12E-01	5.96E-05	7.60E-10	6.89E-05
120	1.67E-01	3.70E-05	4.86E-10	2.82E-05
140	1.83E-01	4.44E-05	5.57E-10	3.70E-05
160	2.50E-01	8.29E-05	8.62E-10	8.86E-05
180	2.68E-01	9.53E-05	9.75E-10	1.13E-04
Average S_E		**5.38E-05**	**Average S_H**	**5.18E-05**

Since the conducted power during the MPE measurement was 123 W the calculated power density was then scaled up for 61.5 W radiated power (taking into account 50% talk time). This model does not include the mismatch loss, loss in the cable and finite conductivity of the car surface and as represents a conservative model for exposure assessment. The scaled-up power density values for 61.5 W radiated power are 5.25 W/m^2 (E), and 5.06 W/m^2 (H), that correspond to 0.52 mW/cm^2 (E), and 0.51 mW/cm^2 (H). Measurements yielded average power density of 0.204 mW/cm^2 (E), which shows that the calculated power density is overestimated. The following graph shows a comparison between the measured power density and the simulated one, based on E or H fields, normalized to 61.5 W radiated power.

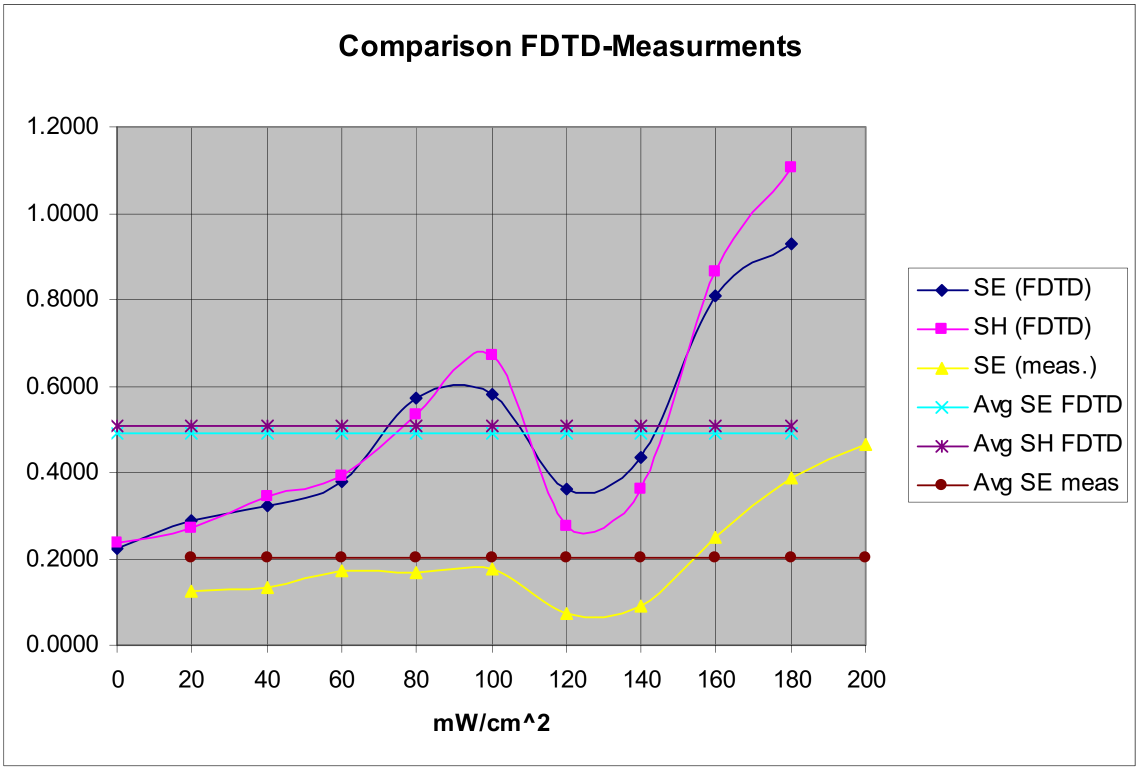

7) Test device positioning

a) A description of the device test positions used in the SAR computations is provided in the SAR report.

b) Illustrations showing the separation distances between the test device and the phantom for the tested configurations are provided in the SAR report.

8) Steady state termination procedures

a) The criteria used to determine that sinusoidal steady-state conditions have been reached throughout the computational domain for terminating the computations are based on the monitoring of field points to make sure they converge. The simulation projects were set to automatically track the field values throughout computational domain by means of XFDTD simulation control feature which ensures that "*convergence is reached when near-zone data shows a constant amplitude sine wave – when all transients have died down and the only variation left is sinusoidal. In this case "convergence" is tested on the average electric field in the space for its deviation from a pure sine wav. XFDTD automatically places points throughout the space for this purpose*." [XFDTD Reference Manual, version. 6.4]. This convergence threshold was set to -40 dB.
In addition for at least one passenger and one bystander exposure condition, we placed one "field sensor" near the antenna, others between the body and the domain boundary at different locations, and one inside the head of the model. In all simulations, isotropic E-field sensors were placed at opposite corners of the computational domain. We used isotropic E and H field "sensors", meaning that all three components of the fields are monitored at these points. The following figures show an example of the time waveforms at the field point sensors in the in two opposite points in the computational domain. We selected points near the lowest and highest grid index points. They are shown together in the figure. The highest field levels are observed for the higher index point, as it is closer to the antenna. In all cases, the field reaches the steady-state after a few cycles.

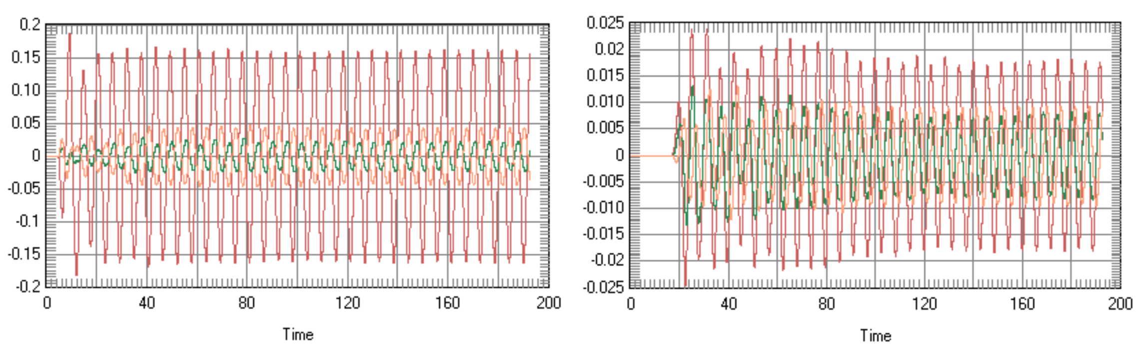

c) The XFDTD™ algorithm determines the field phasors by using the so-called "two-equations two-unknowns" method. Details of the algorithm are explained in [7].

9) Computing peak SAR from field components

a) The twelve E-field phasors at the edges of each Yee voxel are combined to yield the SAR associated to that voxel. In particular, the average is performed on the SAR values computed at the 12 edges of each voxel. Notice that in XFDTD™ the dielectric tissue properties are assigned to the voxel edges, thereby allowing said averaging procedure.

b) The IEEE Standards Coordinating Committee 34, Sub-Committee 2 draft standard P1529 (June 2000) discusses several algorithms for volumetric SAR averaging. It states that "It is observed that while the 12 components algorithm is the most appropriate from the mathematical point of view, the differences in 1g SAR calculated with either the 12 or 6 component methods are negligible for practical mesh resolutions (below 5mm). On the other hand, it is shown that the 3 components approach may lead to significant errors." XFDTD™ employs the 12-component method, which is the one recommended in the draft standard, thus providing the best achievable accuracy.

10) One-gram averaged SAR procedures

a) XFDTD™ computes the Specific Absorption Rate (SAR) in each complete cell containing lossy dielectric material and with a non-zero material density. To be considered a complete cell, the twelve cell edges must belong to lossy dielectric materials. The averaging calculation uses an interpolation scheme for finding the averages. Cubical spaces centered on a cell are formed and the mass and average SAR of the sample cubes are found. The size of the sample cubes increases until the total mass of the enclosed exceeds either 1 or 10 grams. The mass and average SAR value of each cube is saved and used to interpolate the average SAR values at either 1 or 10 grams. The interpolation is performed using two methods (polynomial fit and rational function fit) and the one with the lowest error is chosen. The sample cube must meet some conditions to be considered valid. The cube may contain some non-tissue cells, but some checks are performed on the distribution of the non-tissue cells. A valid cube will not contain an entire side or corner of non-tissue cells.

b) The sample cube increases in odd-numbered steps (1x1x1, 3x3x3, 5x5x5, etc) to remain centered on the desired cell. Since the visible human model employed herein has 5 mm resolution, the one-gram SAR is computed by averaging first over 1x1x1 voxels, corresponding to 0.125 cm^3 (not enough yet), and then over a 3x3x3 voxel cube, corresponding to about 3.4 cm^3, which is enough to include 1-g, and finally over a 5x5x5 voxel cube, corresponding to about 15.6 cm^3, which includes 10-g. The 1-g average SAR is computed by interpolating these three data points. This procedure is repeated in the surroundings of each voxel that is constituted by lossy materials, so as to determine the 1-g and/or 10-g SAR distributions.

c) As mentioned at points 10(a) and 10(b), the 1- gram average SAR is determined by interpolating the average SAR for the 1x1x1 , 3x3x3, and the 5x5x5 data points, corresponding to 0.125 cm^3, 3.4 cm^3, and 15.6 cm^3, respectively. Because the interpolation is carried out across three data points, the error introduced should be negligible because the interpolating curve crosses exactly the data points.

11) Total computational uncertainty – We derived an estimate for the uncertainty of FDTD methods in evaluating SAR by referring to [6]. In Fig. 7 in [6] it is shown that the deviation between SAR estimates using the XFDTD™ code and those measured with a compliance system are typically within 10% when the probe is away from the phantom surface so that boundary effects are negligible. In that example, the simulated SAR always exceeds the measured SAR.

As discussed in 6(a), a conservative bias has been introduced in the model so as to reduce concerns regarding the computational uncertainty related to the car modeling, antenna modeling, and phantom modeling. The results of the comparison between measurements and simulations presented in 6(a) suggest that the present model produces an overestimate of the exposure between 4% and 36%. Such a conservative bias should eliminate the need for including uncertainty considerations in the SAR assessment.

12) Test results for determining SAR compliance

a) Illustrations showing the SAR distribution of dominant peak locations produced by the test transmitter, with respect to the phantom and test device, are provided in the SAR report.

b) The input impedance and the total power radiated under the impedance match conditions that occur at the test frequency are provided by XFDTD™. XFDTD™ computes the input impedance by following the method outlined in [8], which consists in performing the integration of the steady-state magnetic field around the feed point edge to compute the steady-state feed point current (*I*), which is then used to divide the feed-gap steady-state voltage (*V*). The net average radiated power is computed as

$$P_{XFDTD} = \frac{1}{2}\mathrm{Re}\left\{VI^*\right\}$$

Both the input impedance and the net average radiated power are provided by XFDTD™ at the end of each individual simulation.

We normalize the SAR to such a power, thereby obtaining SAR per radiated Watt (*normalized SAR*) values for the whole body and the 1-g SAR. Finally, we multiply such normalized SAR values times the max power rating of the device under test. In this way, we obtain the exposure metrics for 100% talk-time, i.e., without applying source-based time averaging.

c) For mobile radios, 50% source-based time averaging is applied by multiplying the SAR values determined at point 12(b) times a 0.5 factor.

REFERENCES

[1] K. S. Yee, "Numerical Solution of Initial Boundary Value Problems Involving Maxwell's Equations in Isotropic Media," *IEEE Transactions on Antennas and Propagation*, vol. 14, no. 3, 302-307, March 1966.

[2] Z. P. Liao, H. L. Wong, G. P. Yang, and Y. F. Yuan, "A transmitting boundary for transient wave analysis," Scientia Sinica, vol. 28, no. 10, pp 1063-1076, Oct. 1984.

[3] Validation exercise: Mie sphere. Remcom Inc. (enclosed PDF)

Remcom.pdf

[4] NEC-Win PRO ™ v 1.1, Nittany Scientific, Inc., Riverton, UT.

[5] C. M. Collins and M. B. Smith, "Calculations of B1 distribution, SNR, and SAR for a surface coil against an anatomically-accurate human body model," *Magn. Reson. Med.*, 45:692-699, 2001. (enclosed TIF)

Collins & Smith.pdf

[6] Martin Siegbahn and Christer Törnevik, "Measurements and FDTD Computations of the IEEE SCC 34 Spherical Bowl and Dipole Antenna," Report to the IEEE Standards Coordinating Committee 34, Sub-Committee 2, 1998. (enclosed PDF)

Ericsson.pdf

[7] C. M. Furse and O. P. Gandhi, "Calculation of electric fields and currents induced in a millimeter-resolution human model at 60 Hz using the FDTD method with a novel time-to-frequency-domain conversion**,"** Antennas and Propagation Society International Symposium, 1996. (enclosed PDF)

Furse & Gandhi.pdf

[8] *The Finite Difference Time Domain Method for Electromagnetics*, Chapter 14.2, by K. S. Kunz and R. J. Luebbers, CRC Press, Boca Raton, Florida, 1993.

[9] *Validation of Mobile Antenna Modeling by Comparison with Near-field Measurements*," Report to the IEEE Standards Coordinating Committee 34, Sub-Committee 2, 2006. (enclosed PDF)

IEEE1528_2_vld.pdf

[10] *Antenna Theory: analysis and design,* Chapter 4, by C. A. Balanis, 2nd ed. John Wiley & Sons, Inc.